

New result for the neutron β -asymmetry parameter A_0 from UCNA

M. A.-P. Brown,¹ E. B. Dees,^{2,3} E. Adamek,⁴ B. Allgeier,¹ M. Blatnik,⁵ T. J. Bowles,⁶ L. J. Broussard,^{6,*}
 R. Carr,⁵ S. Clayton,⁶ C. Cude-Woods,² S. Currie,⁶ X. Ding,⁷ B. W. Filippone,⁵ A. García,⁸ P. Geltenbort,⁹
 S. Hasan,¹ K. P. Hickerson,⁵ J. Hoagland,² R. Hong,⁸ G. E. Hogan,⁶ A. T. Holley,^{2,4,†} T. M. Ito,⁶ A. Knecht,^{8,‡}
 C.-Y. Liu,⁴ J. Liu,¹⁰ M. Makela,⁶ J. W. Martin,^{5,11} D. Melconian,¹² M. P. Mendenhall,^{5,§} S. D. Moore,²
 C. L. Morris,⁶ S. Nepal,¹ N. Nouri,^{1,¶} R. W. Pattie, Jr.,^{2,3} A. Pérez-Galván,^{5,**} D. G. Phillips II,² R. Picker,^{5,††}
 M. L. Pitt,⁷ B. Plaster,¹ J. C. Ramsey,⁶ R. Rios,^{6,13} D. J. Salvat,⁸ A. Saunders,⁶ W. Sondheim,⁶
 S. J. Seestrom,⁶ S. Sjue,⁶ S. Slutsky,⁵ X. Sun,⁵ C. Swank,⁵ G. Swift,³ E. Tatar,¹³ R. B. Vogelaar,⁷
 B. VornDick,² Z. Wang,⁶ J. Wexler,² T. Womack,⁶ C. Wrede,^{8,14} A. R. Young,^{2,3} and B. A. Zeck²

(UCNA Collaboration)

¹Department of Physics and Astronomy, University of Kentucky, Lexington, Kentucky 40506, USA

²Department of Physics, North Carolina State University, Raleigh, North Carolina 27695, USA

³Triangle Universities Nuclear Laboratory, Durham, North Carolina 27708, USA

⁴Department of Physics, Indiana University, Bloomington, Indiana 47408, USA

⁵W. K. Kellogg Radiation Laboratory, California Institute of Technology, Pasadena, California 91125, USA

⁶Los Alamos National Laboratory, Los Alamos, New Mexico 87545, USA

⁷Department of Physics, Virginia Tech, Blacksburg, Virginia 24061, USA

⁸Department of Physics and Center for Experimental Nuclear Physics and Astrophysics,
University of Washington, Seattle, Washington 98195, USA

⁹Institut Laue-Langevin, 38042 Grenoble Cedex 9, France

¹⁰Department of Physics, Shanghai Jiao Tong University, Shanghai, 200240, China

¹¹Department of Physics, University of Winnipeg, Winnipeg, MB R3B 2E9, Canada

¹²Cyclotron Institute, Texas A&M University, College Station, Texas 77843, USA

¹³Department of Physics, Idaho State University, Pocatello, Idaho 83209, USA

¹⁴Department of Physics and Astronomy and National Superconducting Cyclotron Laboratory,
Michigan State University, East Lansing, Michigan 48824, USA

(Dated: December 5, 2017)

The neutron β -decay asymmetry parameter A_0 defines the correlation between the spin of the neutron and the momentum of the emitted electron, which determines $\lambda = \frac{g_A}{g_V}$, the ratio of the axial-vector to vector weak coupling constants. The UCNA Experiment, located at the Ultracold Neutron facility at the Los Alamos Neutron Science Center, is the first to measure such a correlation coefficient using ultracold neutrons (UCN). Following improvements to the systematic uncertainties and increased statistics, we report the new result $A_0 = -0.12054(44)_{\text{stat}}(68)_{\text{syst}}$ which yields $\lambda \equiv \frac{g_A}{g_V} = -1.2783(22)$. Combination with the previous UCNA result and accounting for correlated systematic uncertainties produces $A_0 = -0.12015(34)_{\text{stat}}(63)_{\text{syst}}$ and $\lambda \equiv \frac{g_A}{g_V} = -1.2772(20)$.

Precision measurements of A_0 , the correlation between the electron momentum and the initial spin of the neutron in neutron β -decay, remain vital as they determine with highest sensitivity $\lambda \equiv \frac{g_A}{g_V}$, the ratio of the weak axial-vector to vector coupling constants present in the hadronic current. Although a_0 , the correlation between the electron momentum and the neutrino momentum,

and A_0 offer comparable sensitivity to λ , measurements of a_0 require the difficult task of reconstruction of the neutrino momentum via detection of electron-proton coincidences [1] or measurement of the proton energy spectrum [2]. Under assumption of the Conserved Vector Current (CVC) hypothesis, experimentally determined values for λ directly determine g_A . This serves as a benchmark for lattice QCD calculations and determines the relationship among parameters of the weak hadronic current. Recent improvements in lattice QCD calculations [3–5] show promising agreement between theory and experiment, and thus further motivate precision measurements of neutron correlation parameters. Also, results for λ when combined with results for the neutron lifetime permit a test of the standard model [6, 7] via, for example, an extraction of the CKM matrix element V_{ud} .

The decay rate of polarized neutrons can be written in a simplified manner as [8]

$$dW = \Gamma(E_e) \left(1 + \langle P \rangle A(E_e) \beta \cos \theta \right) dE_e d\Omega_e \quad (1)$$

* Currently at Oak Ridge National Laboratory, Oak Ridge, TN 37831, USA

† Currently at Dept. of Physics, Tennessee Tech University, Cookeville, TN, USA

‡ Currently at Paul Scherrer Institut, 5232 Villigen PSI, Switzerland

§ Currently at Physical and Life Sciences Directorate, Lawrence Livermore National Laboratory, Livermore, CA 94550, USA

¶ Currently at Department of Pathology, Yale University School of Medicine, New Haven, Connecticut 06510, USA

** Currently at Vertex Pharmaceuticals, 11010 Torreyana Rd., San Diego, CA 92121, USA

†† Currently at TRIUMF, Vancouver, BC V6T 2A3 Canada

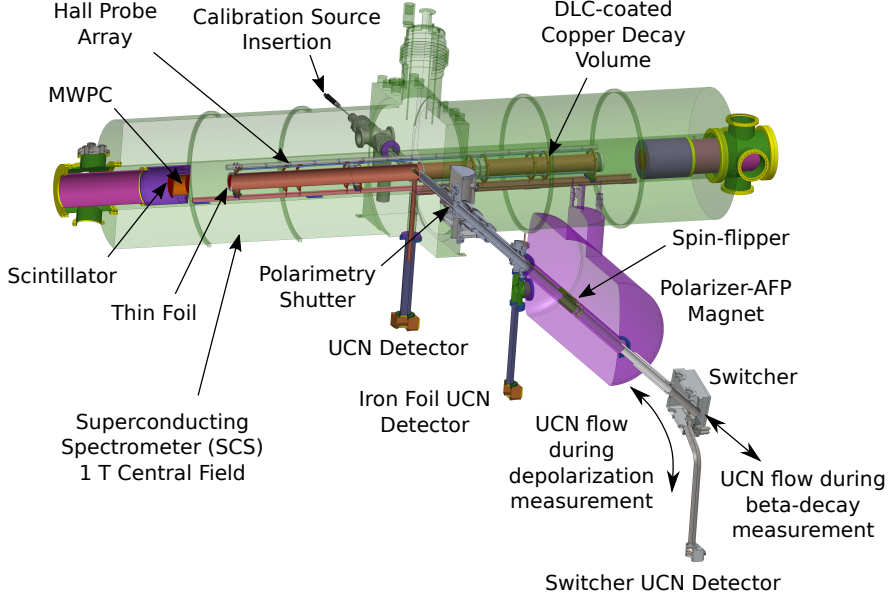


FIG. 1. Schematic of the UCNA experimental apparatus. The external muon veto and “backing veto” are not pictured.

where $\Gamma(E_e)$ is the unpolarized neutron differential decay rate, $\langle P \rangle$ is the average polarization, $\beta = \frac{v}{c}$, v is the electron velocity, θ is the angle between the neutron spin and the emitted electron momentum, and $A(E)$ is the energy dependent asymmetry parameter [9, 10]. Neglecting corrections from recoil order and radiative effects, $A(E_e)$ may be expressed as A_0 , where [8]

$$A_0 = \frac{-2(\lambda^2 - |\lambda|)}{1 + 3\lambda^2}. \quad (2)$$

The UCNA Experiment, located at the Los Alamos Neutron Science Center, is the first to measure a neutron angular correlation coefficient using ultracold neutrons (UCN). The 800 MeV LANSCE linear accelerator strikes a tungsten spallation target. The resulting spallation neutrons are moderated by cold polyethylene, and are subsequently down-scattered to UCN energies by a solid ortho-deuterium crystal [11]. The UCN are guided through a 7 T polarizing magnet and through an Adiabatic Fast Passage (AFP) spin flipper [12] allowing for selection of either + (spin flipper “on”) or – (spin flipper “off”) spin states. The UCN, held within a 3 m long superconducting spectrometer (SCS) [13], have spins aligned (+) or anti-aligned (–) with a 1 T field about which the decay electrons spiral while heading towards one of two detectors placed at each end of the SCS. The electron detector packages consist of a multiwire proportional chamber (MWPC) [14] for position reconstruction and backscattering identification and a plastic scintillator for timing and energy reconstruction. We also detect background muons using a combination of plastic scintillator paddles and Ar/ethane drift tubes [15] and

15 cm diameter, 25 mm thick scintillators placed directly behind the electron detectors (the “backing veto”). A schematic of the experimental apparatus is presented in Fig. 1.

In this work, we present a more precise determination of the average polarization of the neutrons in the decay volume, a new method for quantifying the uncertainty in energy reconstruction, and a more robust determination of the systematic uncertainties from Monte Carlo corrections to the electron detector response. These improvements coupled with better statistics reduce the overall uncertainty relative to previous UCNA results [16–19].

UCNA utilizes a run-by-run monitor of the depolarization of the neutron populations in the decay volume, with a statistics-limited uncertainty in the extracted polarization [12, 16–19]. For this work, we present an update of our polarimetry method based on the implementation of a shutter between the decay volume and polarizer/AFP magnet (see Fig. 1), with further details in preparation as a forthcoming publication. Our methodology for preparing the spin state is essentially identical to previous versions of the experiment, in that the UCN are first polarized by traversing a 7 T magnetic field region. The potential energy barrier to the low field-seeking spin state ensures UCN are essentially 100% polarized immediately after passing through this region. Beyond the high-field region, the adiabatic spin flipper is used to select the spin state loaded into the decay volume, operating with single-pass spin-flip efficiency in excess of 99.9%.

The run-cycle was composed of a 50 min interval in which beta decay data was obtained with neutrons prepared in a given spin state (the spin state for successive

runs alternates in such a way so as to cancel linear drifts in subtracted backgrounds and detector efficiencies [17]), followed by a procedure to measure the equilibrium population of depolarized UCN in the decay volume. This “*in situ*” procedure utilized the shutter to store UCN in the decay volume while guides were emptied of UCN, and a UCN detector located below the switcher to measure the depolarized UCN. Because the polarization is close to unity, it is sufficient for us to measure the depolarized fraction with modest precision. For the results we present here, our measured polarization is independent of detector efficiencies and UCN transport to first order. The results of our polarimetry measurements for the 2011-2012 and 2012-2013 run-cycles are presented in Table I, with a more detailed overview of our polarimetry analysis presented in Appendix I.

TABLE I. Results for average polarization fractions for each dataset in spin-flipper off (−) and spin-flipper on (+) states.

2011-2012		2012-2013	
P^-	P^+	P^-	P^+
0.9970(30)	0.9939(25)	0.9979(15)	0.9952(20)

The β -decay data were separated into 2011-2012 and 2012-2013 datasets. There were minor changes in spectrometer design between the two run periods, most notably the use of 130 nm and 180 nm 6F6F thick [20] decay trap foils on the East and West sides respectively in 2012-2013, which replaced 500 nm thick Mylar foils used in 2011-2012, all of which were coated with 150 nm thick layer of Beryllium. Such changes affect the backscattering of the electrons and angular acceptance of the detectors, which allows for further exploration of the systematic effects from the decay trap foils, a leading uncertainty in past analyses. This required separate simulations of both calibration and β -decay data, calling for development of separate Monte Carlo systematic corrections and energy uncertainties for each dataset. The resulting electron energy spectrum averaged over both datasets can be seen in Fig. 2 along with the Monte Carlo spectrum and the subtracted background distribution, with the residuals between the Monte Carlo spectrum and data plotted underneath.

The detector calibration for the current result begins with pedestal subtraction and removal of time dependent gain fluctuations as measured by a ^{207}Bi gain monitoring system [21]. We then determine the position dependent light transport of each scintillator during several periods of each run cycle by filling the decay volume with neutron activated xenon gas and fitting the endpoint of the ^{135}Xe $\frac{3}{2}^+$ beta-decay spectrum in position bins determined using the MWPC. Then the position dependent response factors are calculated by normalizing the response in each position bin to the response at the center of the scintillator. Upon correction of the position dependence, we utilize the conversion electron lines

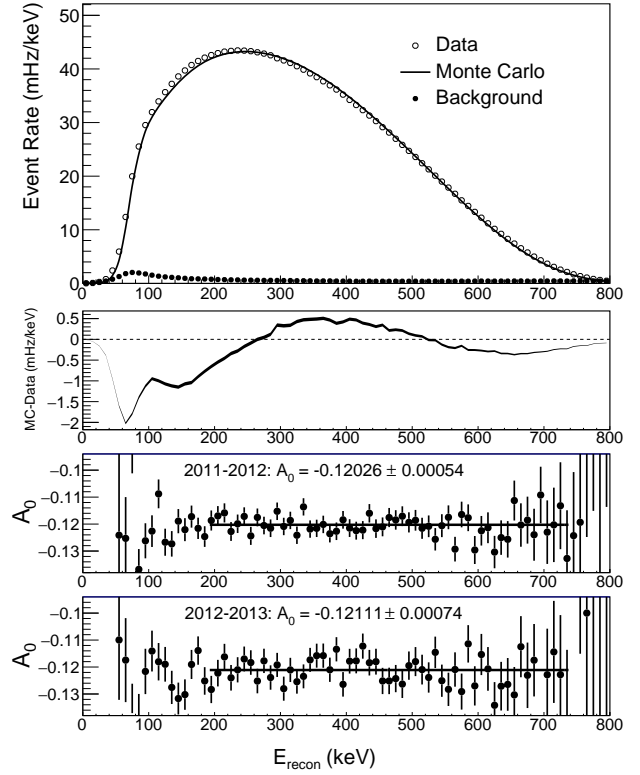


FIG. 2. Top: Electron energy spectrum from 2011-2013 with background-subtracted data (open circles), Geant4 Monte Carlo (solid line), and background (solid circles) included. Residuals between Monte Carlo and data are below. Bottom: Fully corrected asymmetry as a function of energy for the two separate run periods. The fit is over 190-740 keV, as determined via minimization of the total uncertainty. The errors on the indicated fitted values are purely statistical.

from (with dominant K-shell energies listed) ^{137}Ce (130.3 keV), ^{113}Sn (363.8 keV), and ^{207}Bi (481.7 keV and 975.7 keV) sources. At intermittent periods during the run cycle, these sources were translated in a calibration fixture inserted through a side port in the SCS across the detector face, providing a linearity mapping from detector response to expected light output as provided by simulation of each run. Combination of the linearity mapping and the position dependent light transport values converts detector ADC response to reconstructed electron energy, E_{recon} [17].

Upon completion of the calibration procedure, we then analyze each of the conversion electron source runs using these calibrations to determine a reconstructed peak energy. Concurrently we apply the detector response model to simulations of these conversion electron runs, and from this extract a simulated reconstructed energy. A comparison of the reconstructed energies from data and simulation in the form of a residual (Residual = $E_{\text{data}} - E_{\text{MC}}$) then provides a measure of the efficacy of our calibration procedure at the discrete conversion electron energies, which are the points plotted in Fig. 3. The error bands

in Fig. 3 represent our assessment of the accuracy to which we reconstruct the initial energy of an event as a continuous function of the true initial energy, where the error band is determined by allowing for all quadratic calibration curves which could produce the 1σ residuals extracted from calibration of the source runs [22]. This method inherently yields an asymmetric error band due to the residuals being nonzero, so the worst case uncertainty as shown in the figure is one where at every energy the largest deviation from zero residual is taken and plotted symmetrically about the zero residual line. When weighted by the observed β -decay electron energy spectrum, following the edge of the energy uncertainty curve produces fractional uncertainties on A_0 of 0.17% and 0.25% for 2011-2012 and 2012-2013 respectively, with the difference attributed mainly to the offset of the ^{113}Sn peak reconstruction which causes the energy uncertainty band to broaden in the region of our final energy analysis window.

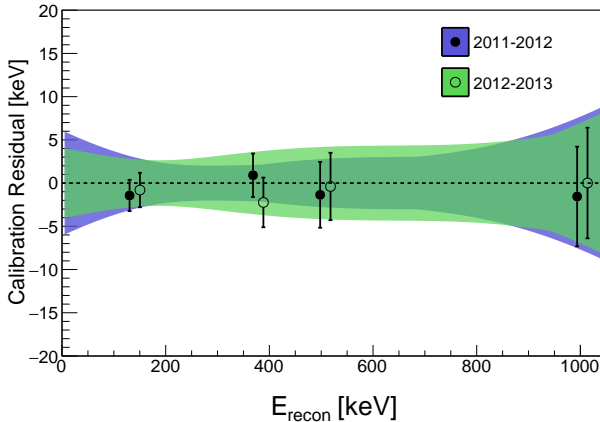


FIG. 3. Plot of energy uncertainty vs. reconstructed energy. The points plotted are the mean and σ of the residual distributions from reconstructed calibration peaks of Ce, Sn, and the lower and upper Bi peaks in that order. The bands represent the energy uncertainty at any given electron energy for the two data sets.

Backscattering identification plays an important role in our Monte Carlo corrections and asymmetry extraction. Based on which detector components trigger, we classify events into those that do not backscatter (Type 0) and those that do backscatter (Types 1, 2, and 3) [17]. Type 0 events trigger one scintillator and one MWPC on the same side, while Type 1 events trigger both scintillators and both MWPCs. For such events, we assign the initial direction to the triggering detector for Type 0 and to the earlier triggering detector for Type 1. Type 2/3 events comprise a class of events that backscatter and trigger both MWPCs, but only trigger a single scintillator. An important distinction, however, does exist between Type 2 and Type 3 events: Type 2 events only pass through the MWPC on the triggering scintillator side once, whereas Type 3 events scatter from the scin-

tillator, and therefore pass through the MWPC twice on the triggering side. We can consequently apply a cut on the energy deposited in the MWPC on the triggering side to statistically assign Type 2/3 events to the correct side. This drastically reduces Monte Carlo corrections for such backscattering events as simulation indicates we properly identify $> 80\%$ of all Type 2/3 events across all energies using this technique, a marked improvement over the roughly 50% misidentification rate without separation.

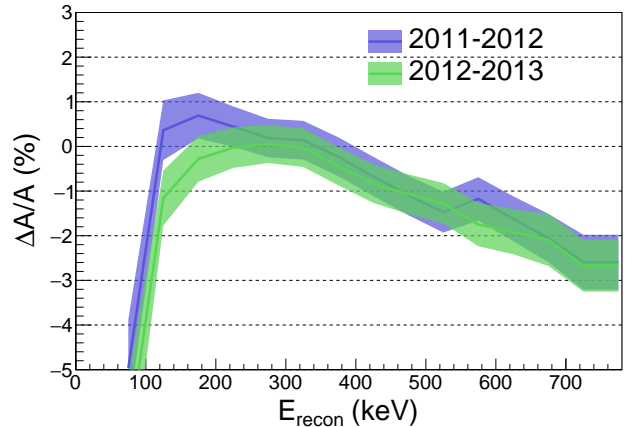


FIG. 4. Total Monte Carlo corrections vs. energy, where $\Delta_{\text{backscatter}}$ and $\Delta_{\cos\theta}$ have been combined. The correction has been averaged over 50 keV increments for plotting purposes, while the correction is actually applied on a 10 keV bin basis. The uncertainty band reflects the effective statistical fluctuations on a bin-by-bin basis, as well as the true Monte Carlo statistical uncertainty and the uncertainty on the correction as determined by spectral agreement between data and simulation for each event type.

With much improved energy reconstruction and depolarization uncertainties, we revisited the conservative 25% uncertainty on the Monte Carlo corrections from the previous analysis [16–19] in search of a more quantitative method. Our systematic corrections take the form $A^{\text{corr}} = (1 + \Delta)A$, where a measured asymmetry A is corrected for some systematic effect Δ . The energy-dependent Monte Carlo correction consists of a missed backscattering correction, $\Delta_{\text{backscatter}}$, and what we call the $\cos\theta$ correction, $\Delta_{\cos\theta}$. The missed backscattering correction accounts for events that are assigned the wrong initial direction based on the detector trigger logic, a result of either the efficiency of the detector or backscattering from components not part of the detectors. Application of this correction increases the magnitude of the asymmetry, as the misidentified backscattering events act as a dilution to the measured asymmetry. The $\cos\theta$ correction addresses experimental bias towards high energy, low pitch angle events, which are more apt to trigger the detectors. The correction is named for the deviation of $\langle \cos\theta \rangle$ over one hemisphere of the spectrometer from its nominal value of 1/2. Because low pitch angle, high energy events carry more asymmetry infor-

mation as seen in Eq. 1, preferentially selecting them will increase the measured asymmetry, thus the $\Delta_{\cos\theta}$ correction acts to reduce the magnitude of the measured asymmetry. The improvement in quantifying the uncertainty in Monte Carlo corrections results from work done to separate both $\Delta_{\text{backscatter}}$ and $\Delta_{\cos\theta}$ into their relative contributions from each individual event type, such that $(1 + \Delta_{\text{backscatter}}) = \prod_{i=0}^3 (1 + \Delta_{\text{backscatter},i})$ and similarly for the $\cos\theta$ correction, where the subscript i runs over all event types. Then, for each event type, we conservatively apply the maximal spectral deviations between Monte Carlo and data within the final analysis energy window in conjunction with an effective statistical fluctuation in the corrections as the contribution to the total uncertainty. The effective statistical uncertainty comes from a functional fit to the binned correction, where the RMS between the correction and the fit defines the uncertainty. One should note that the actual Monte Carlo statistical uncertainties are also included, but they are small relative to the correction and did not account for bin-by-bin variations in the correction. These individual contributions can be further propagated into a single uncertainty on $\Delta_{\text{backscatter}}$ and $\Delta_{\cos\theta}$. Fig. 4 shows the combined corrections for $\Delta_{\text{backscatter}}$ and $\Delta_{\cos\theta}$ for each data set. While the final uncertainty on the combined Monte Carlo corrections is consistent with the uncertainty from the previous UCNA result [16], this method allows for improved understanding of individual contributions to the overall uncertainty.

TABLE II. Uncertainty Table reported as % correction on $|A_0|$. The uncertainties reported are the combined uncertainties from the two data sets as determined based on the respective weights of each data set and treating the systematic uncertainties from the two years as correlated.

	% Corr. 2011-2012	% Unc. 2012-2013
$\Delta_{\cos\theta}$	-1.53	-1.51
$\Delta_{\text{backscattering}}$	1.08	0.88
Energy Recon.		0.20
Depolarization	0.45	0.34
Gain		0.16
Field Nonunif.		0.12
Muon Veto		0.03
UCN Background	0.01	0.01
MWPC Efficiency	0.13	0.11
Statistics		0.36
Theory Corrections [9, 10, 24–27]		
Recoil Order	-1.68	-1.67
Radiative	-0.12	-0.12

The asymmetry was extracted using a super-ratio technique utilizing counts in each detector for spin flipped configurations, defined as

$$A_{\text{SR}} = \frac{1 - \sqrt{R}}{1 + \sqrt{R}} = \langle P \rangle A(E_e) \beta \langle \cos \theta \rangle \quad (3)$$

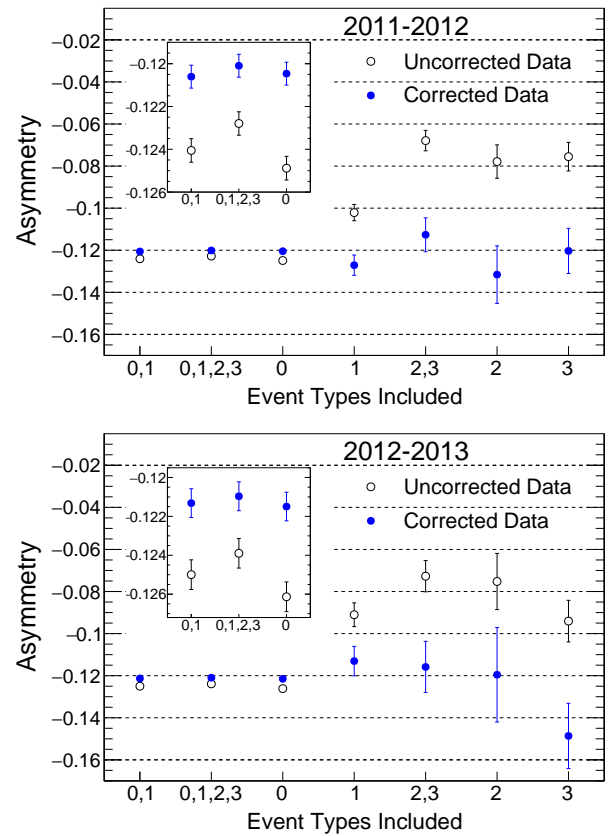


FIG. 5. Corrected and uncorrected asymmetries for various combinations of event types. Only $\Delta_{\text{backscattering}}$ and $\Delta_{\cos\theta}$ are applied and error bars are statistical only. The first three combinations include Type 0 events which are identified as having not backscattered and make up roughly 95% of the data. The remaining four asymmetries include only the various backscattering events. The inset shows a closer view of the first three points whose error bars are smaller than the markers in the larger plot. Top: 2011-2012. Bottom: 2012-2013.

where $R = (r_1^+ r_2^-)/(r_2^+ r_1^-)$ and $r_{1,2}^\pm$ refers to the rate in one of the two detectors (subscript 1, 2) with spin-flipper on/off (superscript +/−). Separating the data into 10 keV energy bins, we divide out β , $\langle P \rangle$, and $\langle \cos \theta \rangle$ and subsequently apply Monte Carlo corrections from Fig. 4 and radiative and recoil order theory corrections [9, 10, 24–27], which produces A_0 as a function of energy as seen in Fig. 2. The analysis was blinded using altered time stamps which are spin-state and detector dependent and do not cancel in the super-ratio. This requires using two blinding factors, $f_{1,2}$, such that $t_{1,2}^\pm = (1 \pm f_{1,2}) \cdot t$ where t is the global time and $t_{1,2}^\pm$ are the blinded times for each detector in each spin state. We completed detector calibrations, all systematic corrections, and the polarimetry analysis prior to unblinding, at which point all rates were recalculated using the proper global time t , generating the asymmetries reported in Fig. 2.

For the asymmetry as reported here, we utilized all

event types (0, 1, 2, and 3 with 2 and 3 separated using the aforementioned MWPC energy deposition) subject to a fiducial cut selecting events within 50 mm of the center of the decay trap. The fiducial cut removes events that could have potentially interacted with the decay trap wall, as the maximum radius of the electron's spiral around the magnetic field is 7.76 mm and the wall of the decay trap is 62.2 mm from the center. Inclusion of any combination of the aforementioned event types yields separate asymmetries, as can be seen in Fig. 5. The agreement between the asymmetries extracted using non-backscattering events (Type 0) and backscattering events only (Types 1, 2, or 3) highlights the credence of the Monte Carlo corrections for backscattering.

The systematic errors for the two data sets are listed in Table II. The asymmetries from 2011-2012 and 2012-2013 are combined to produce a single result utilizing a weighting method [23] that considers the statistics of each result and treats the systematics as completely correlated, producing weights for the 2011-2012 and 2012-2013 asymmetries of 0.67 and 0.33 respectively. Fitting over an analysis window of 190-740 keV, which minimizes the total uncertainty, yields $A_0 = -0.12054(44)_{\text{stat}}(68)_{\text{syst}}$ corresponding to a value for the ratio of the axial-vector to vector coupling constants of $\lambda \equiv \frac{g_A}{g_V} = -1.2783(22)$, where the statistical and systematic uncertainties have been added in quadrature.

We also report a combined result using our previous measurement [16] and a similar weighting method as above, where all systematic uncertainties were set to the smallest reported value between the two measurements and treated as completely correlated so as to avoid artificially small combined systematic uncertainties. We obtain the values $A_0 = -0.12015(34)_{\text{stat}}(63)_{\text{syst}}$ and $\lambda \equiv \frac{g_A}{g_V} = -1.2772(20)$, with weights of 0.39 for the previous result [16] and 0.61 for the result from this analysis.

As shown in Fig. 6, one can constrain V_{ud} using λ [16, 38–44] and neutron lifetime measurements [29–36] and compare to direct measurements of V_{ud} from $0^+ \rightarrow 0^+$ superallowed decays [37]. When considering the discrepancy between neutron lifetime measurements using neutron beams [29, 30] versus UCN storage experiments (performed with material bottles [32–36] and magnetic bottles [31]) and the shift in λ measurements after 2002, one observes a striking landscape. The older pre-2002 results contribute significantly to the χ^2 of the entire data set, leading the Particle Data Group (PDG) to apply a $\sqrt{\chi^2/(N-1)} = 2.2$ scale factor to the current λ error [37]. A common theme between the majority of the pre- and post-2002 results for λ concerns the size of the systematic corrections, where the pre-2002 measurements ([38–40]) have individual systematic corrections $> 10\%$ compared to those from post-2002 ([16, 41, 42] and this work) with all systematic corrections $< 2\%$. For the future, we note that if the precision level of measurements of the beta asymmetry achieve the roughly 0.1% level required for direct comparison with V_{ud} extracted from

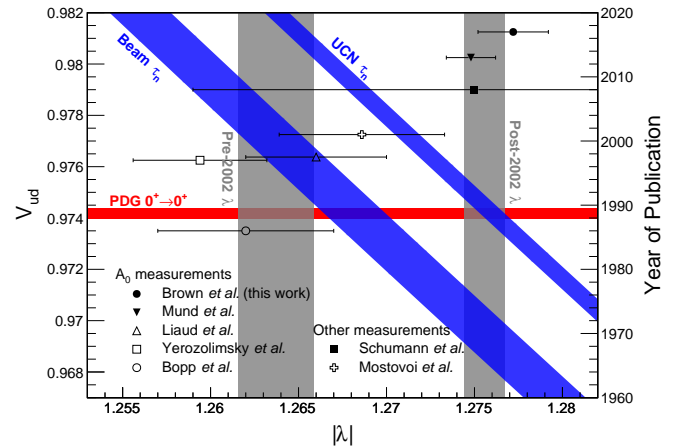


FIG. 6. Status of V_{ud} , the neutron lifetime, and λ measurements. The λ result bands (vertical) are divided into pre-2002 [38–40] and post-2002 [16, 42–44] results, where the distinction is made using the date of the most recent result from each experiment. The right axis shows publication year for the individual lambda measurements included in the calculation of the λ bands (closed markers for post-2002, open markers for pre-2002). Note that the result of this work (Brown *et al.*) is the combined UCNA result from [16] and the current analysis, and the Mund *et al.* result is the combined PERKEOII result from [41, 42]. The diagonal bands are derived from neutron lifetime measurements and are separated into neutron beam [29, 30] and UCN bottle experiments, which consist of material bottle storage [32–36] and magnetic bottle storage [31]. The V_{ud} band (horizontal) comes from superallowed $0^+ \rightarrow 0^+$ nuclear β -decay measurements [37]. The error bands include scale factors as prescribed by the Particle Data Group [37].

$0^+ \rightarrow 0^+$ superallowed decays [45], the pre-2002 measurements will not contribute to the Particle Data Group's scatter calculations for the beta asymmetry, setting the precision level for evaluating scatter and the global averages at the scale of the recent measurements and those to come¹.

This work is supported in part by the U.S. Department of Energy, Office of Nuclear Physics (DE-FG02-08ER41557, DE-SC0014622, DE-FG02-97ER41042) and the National Science Foundation (NSF-0700491, NSF-1002814, NSF-1005233, NSF-1102511, NSF-1205977, NSF-1306997, NSF-1307426, NSF-1506459, and NSF-1615153). We gratefully acknowledge the support of the LDRD program (20110043DR), and the LANSCE and AOT divisions of the Los Alamos National Laboratory.

¹ The PDG only includes in the calculation of the scale factor those measurements that satisfy $\delta x_i < 3\sqrt{N}\delta\bar{x}$, where x_i refers to one measurement of quantity x out of N measurements and $\delta\bar{x}$ is the non-scaled error on the weighted average \bar{x} [37]. Inclusion of a 0.1% result for A_0 (yielding a 0.025% result for λ), removes the pre-2002 results for λ from those that enter the calculation of the scale factor.

I. APPENDIX

During β -decay running, an equilibrium population of spins develops. We characterize this equilibrium spin population by a depolarized fraction at time t , with $t = 0$ s at the beginning of a polarimetry measurement: $\xi(t) = [N_{\text{depol}}(t)/N_{\text{load}}(t)]$, where “load” indicates the equilibrium population of neutron spin states that developed in the decay trap (mainly the spin state chosen by the spin flipper with a small depolarized contribution), and “depol” indicates neutrons which have the opposite spin state (nominally depolarized). The polarization at time t is then $P(t) = 1 - 2\xi(t)$. We determine the fraction of depolarized neutrons in a given β -decay run by performing depolarization or “D” runs at the end of each 50 min. β -decay run. In these runs, the loaded spin populations are determined by direct measurement of the UCN population in the spectrometer decay volume just before the beginning of a depolarization measurement. Because depolarized populations are small (smaller than 1 %), the β -decay rate or the rate in a UCN monitor attached to the SCS is sufficient to provide a reliable measure proportional to the loaded spin population, $N_{\text{load}}^{\text{SCS}}(t = 0 \text{ s})$, where the superscript “SCS” indicates measurement with either the UCN monitor or electron detectors in the β -decay spectrometer.

The depolarized spin population is isolated and measured in a procedure with five steps. In step (1), we utilize a new component for the UCNA experiment: a shutter at the exit of the decay trap (see Fig. 1). The shutter dramatically improves the signal-to-background ratio in our measurement of the depolarized fraction, and permits a very clean assessment of the systematic errors in our polarimetry analysis. At time $t = 0$ s, the shutter is closed, preventing UCN in the decay volume from exiting the system. When the shutter closes, the state of the switcher also changes, routing UCN that exit from the decay trap through the polarizer/AFP magnet to a UCN detector located below the switcher. The signal in the switcher detector during a polarimetry run is depicted in Fig. 7. After the shutter is closed, the loaded spin population in the guides between the shutter and the switcher detector are permitted to drain to the switcher detector, producing a large pulse in the switcher detector. In step (2), at $t = 25$ s, the state of the spin flipper is changed, permitting depolarized UCN in the guides beyond the spin-flipper to also exit to the switcher detector. Note that, prior to this time, the depolarized population is in a state which can not pass the high field region of the polarizer/AFP magnet. In step (3), at time $t = 30$ s, the shutter is opened, permitting only depolarized UCN from the decay trap to traverse the high field region in the polarizer/AFP magnet and be counted in the switcher detector. After background subtraction, the number of UCN counted in this phase by the switcher detector, $N_{\text{depol}}^{\text{SWT}}(t = 30 \text{ s})$, is proportional to the depolarized population at time $t = 30$ s (“SWT” stand for switcher detector). In step (4), at $t = 130$ s, the spin-

flipper is changed again, permitting the initially loaded spin population to drain from the decay trap. Finally, in step (5) at $t = 310$ s, when all UCN have drained from the trap, we take background data in the switcher UCN detector for 50 s.

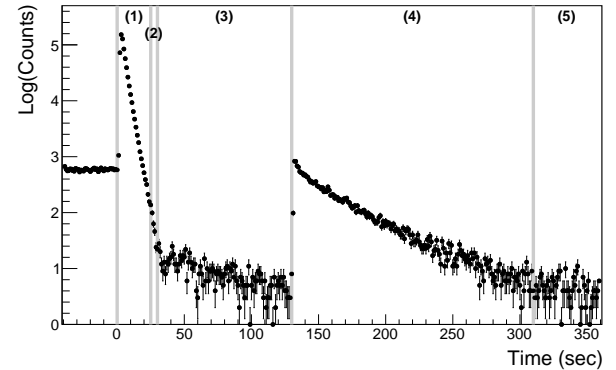


FIG. 7. Switcher signal as a function of time, during “D”-type runs: (1) the shutter closes and the switcher state changes, permitting UCN in the guide outside the decay volume to drain to the switcher UCN detector, (2) the AFP spin-flipper changes state, allowing depolarized neutrons in the guides outside the decay volume to drain to the switcher, (3) the shutter opens, permitting depolarized neutrons within the decay volume to drain to the switcher detector, (4) the AFP spin-flipper returns to its initial state, allowing the initially loaded spin state to drain from the decay volume, (5) backgrounds are measured after the UCN population in the decay volume has drained away. The presented data were taken in 2011 and UCN loaded into the decay volume with the spin-flipper off.

A set of dedicated, “*ex situ*” measurements called “P” runs are performed for both flipper on-loaded and off-loaded UCN to determine the ratio of UCN measured at $t = 0$ s in the SCS to those measured after storing them for 30 s behind the shutter and then unloading them to the switcher detector. This ratio is used (for the spin state corresponding to depolarized UCN in a given D run) to correct the switcher signal measured in the D runs for storage behind the shutter and transport to the switcher. The resultant “raw” depolarized fraction $\xi_{\text{raw}}(t = 0 \text{ s})$ is nominally independent of spin-transport and detection efficiencies.

TABLE III. Results from measured raw depolarization fractions and the range of Monte Carlo correction values for each dataset in spin-flipper off (−) and spin-flipper on (+) states.

	2011-2012		2012-2013	
	P^-	P^+	P^-	P^+
$\xi_{\text{raw}}(t = 0 \text{ s})$	0.0062(4)	0.0099(3)	0.0045(5)	0.0070(3)
MC Corr.	0.15-0.275	0.275-0.375	0.15-0.30	0.25-0.375

A systematic multiplicative correction to the measured value of $\xi_{\text{raw}}(t = 0 \text{ s})$ is determined via Monte Carlo

simulation of the signals in our switcher UCN detector. This correction arises from two effects, the first being that while the depolarized spin population is stored behind the shutter during a D-type run ($t = 0 - 30$ s), it can be continuously fed by depolarization of the initially loaded spin population. We refer to this as the “DE” or depolarization evolution correction, which can affect both flipper-on and flipper-off loaded β -decay runs. The second is due to the finite spin flipper efficiency, and is referred to as the “SFE” correction. This causes a systematic error only for flipper-off loaded runs, because it produces a continuous leakage of UCN from the initially loaded spin population through the spin flipper when the flipper is on (trapping the initially loaded spin population and nominally preventing them from being counted in the switcher detector). Our simulations permit us to systematically explore the guide transport parameters (guide specularity, Fermi potentials, and loss per bounce) as well as the magnitude and correlations

between the DE and SFE corrections. The measured values of $\xi_{\text{raw}}(t = 0 \text{ s})$ and the Monte Carlo correction factors are shown in Table III, and the polarization for the 2011 and 2012 LANL run cycles are tabulated in Table I. The uncertainties for the polarization determined for this work were dominated by the statistical uncertainties in the fitting procedures used to determine the DE and SFE corrections, with these determined by the counting statistics for UCNs in the switcher detector.

The uncertainties for the polarization determined for this work were dominated by the statistical uncertainties in the fitting procedures used to determine the Monte Carlo corrections. In addition to the resultant statistical uncertainty in the Monte Carlo correction factors, we also assigned a 15 % overall systematic uncertainty to the Monte Carlo correction factor due to the worst case disagreement between the switcher signal simulations and Monte Carlo predictions.

-
- [1] G. Darius *et al.*, Phys. Rev. Lett. **119**, 042502 (2017).
- [2] J. Byrne *et al.*, J. Phys. G: Nucl. Part. Phys. **28**, 1325 (2002).
- [3] T. Bhattacharya *et al.*, Phys. Rev. D **94**, 054508 (2016).
- [4] K. Berkowitz *et al.*, “An accurate calculation of the nucleon axial charge with lattice QCD,” (2017), arXiv:1704.01114 [hep-lat].
- [5] S. Capitani *et al.*, “Iso-vector axial form factors of the nucleon in two-flavour lattice QCD,” (2017), arXiv:1705.06186 [hep-lat].
- [6] V. Cirigliano, S. Gardner, and B. Holstein, Prog. Part. Nucl. Phys. **71**, 93 (2013).
- [7] T. Bhattacharya *et al.*, Phys. Rev. D **85**, 054512 (2012)
- [8] J. D. Jackson, S. B. Treiman, and H. W. Wyld Jr. Physical Review **106**, 517 (1957).
- [9] S. Gardner and C. Zhang, Phys. Rev. Lett. **86**, 5666 (2001)
- [10] D. H. Wilkinson, Nucl. Phys. A **377**, 474 (1982)
- [11] A. Saunders *et al.* (UCNA Collaboration), Rev. Sci. Instr. **84**, 013304 (2013).
- [12] A. T. Holley *et al.*, Rev. Sci. Instrum. **83**, 073505 (2012).
- [13] B. Plaster *et al.*, Nucl. Instrum. Methods Phys. Res. A **595**, 587 (2008).
- [14] T. Ito *et al.*, Nucl. Instrum. Methods Phys. Res. A **571**, 676 (2007).
- [15] R. Rios *et al.*, Nucl. Instrum. Methods Phys. Res. A **637**, 105 (2011).
- [16] M. P. Mendenhall *et al.* (UCNA Collaboration), Phys. Rev. C **87**, 032501 (2013).
- [17] B. Plaster *et al.* (UCNA Collaboration), Phys. Rev. A **86**, 055501 (2012).
- [18] R. W. Pattie *et al.* (UCNA Collaboration), Phys. Rev. Lett. **102**, 012301 (2009).
- [19] J. Liu *et al.* (UCNA Collaboration), Phys. Rev. Lett. **105**, 181803 (2010).
- [20] S. Hoedl, “Novel Proton Detectors, Ultra-Cold Neutron Decay and Electron Backscatter,” Ph.D. Thesis, Princeton University, (2003).
- [21] C. L. Morris, W. J. Braithwaite, and C. F. Moore, Nucl. Instrum. Methods **136**, 197 (1976).
- [22] K. P. Hickerson *et al.*, Phys. Rev. C **96**, 042501 (2017).
- [23] M. P. Mendenhall, “Measurement of the neutron beta decay asymmetry using ultracold neutrons,” Ph.D. Thesis, California Institute of Technology, (2014).
- [24] S. M. Bilen’kiĭ *et al.*, Soviet Physics JETP **10**, 1241 (1960), [USSR Vol. 37, pp. 17581763].
- [25] B. R. Holstein, Rev. Mod. Phys. **46**, 789 (1974).
- [26] R. T. Shann, Il Nuovo Cimento **5 A**, 591 (1971).
- [27] F. Glück and K. Tóth, Phys. Rev. D **46**, 2090 (1992)
- [28] W. J. Marciano and A. Sirlin, Phys. Rev. Lett. **96**, 032002 (2006).
- [29] A. T. Yue *et al.*, Phys. Rev. Lett. **111**, 222501 (2013).
- [30] J. Byrne *et al.*, EPL (Europhysics Letters) **33**, 187 (1996).
- [31] R. W. Pattie Jr. *et al.*, “Measurement of the neutron lifetime using an asymmetric magneto-gravitational trap and in situ detection,” (2017), arXiv:1707.01817 [nucl-ex].
- [32] A. Serebrov *et al.*, Phys. Lett. B **605**, 72 (2005).
- [33] S. Arzumanov *et al.*, Phys. Lett. B **745**, 79 (2015).
- [34] A. Steyerl *et al.*, Phys. Rev. C **85**, 065503 (2012).
- [35] A. Pichlmaier *et al.*, Phys. Lett. B **693**, 221 (2010).
- [36] W. Mampe *et al.*, Soviet Physics JETP **57**, 82 (1993).
- [37] C. Patrignani *et al.* (Particle Data Group), Chin. Phys. C **40**, 100001 (2016).
- [38] P. Bopp *et al.*, Phys. Rev. Lett. **56**, 919 (1986).
- [39] B. Yerozolimsky *et al.*, Phys. Lett. B **412**, 240 (1997).
- [40] P. Liaud *et al.*, Nucl. Phys. A **612**, 53 (1997).
- [41] H. Abele *et al.*, Phys. Rev. Lett. **88**, 211801 (2002).
- [42] D. Mund *et al.*, Phys. Rev. Lett. **110**, 172502 (2013).
- [43] M. Schumann *et al.*, Phys. Rev. Lett. **100**, 151801 (2008).
- [44] Y. A. Mostovoi *et al.*, Physics of Atomic Nuclei **64**, 1955 (2001).
- [45] J. C. Hardy and I. S. Towner, Phys. Rev. C **91**, 025501 (2015)